Catalysis Today xxx (xxxx) xxx–xxx

Contents lists available at ScienceDirect

Catalysis Today

journal homepage: www.elsevier.com/locate/cattod

Catalytic reforming of dimethyl ether in microchannels

Cristian Ledesma[a], Eduardo López[a,b], Trifon Trifonov[c], Ángel Rodríguez[d], Jordi Llorca[a,c,e,*]

[a] Institute of Energy Technologies, Universitat Politècnica de Catalunya, EEBE, Eduard Maristany 16, 08019 Barcelona, Spain
[b] Planta Piloto de Ingeniería Química, UNS, CONICET, Camino La Carrindanga km 7, 8000 Bahía Blanca, Argentina
[c] Barcelona Research Center in Multiscale Science and Engineering, Universitat Politècnica de Catalunya, EEBE, Eduard Maristany 16, 08019 Barcelona, Spain
[d] Department of Electronic Engineering, Universitat Politècnica de Catalunya, Campus Nord, Jordi Girona 1-3, 08034 Barcelona, Spain
[e] Department of Chemical Engineering, Universitat Politècnica de Catalunya, EEBE, Eduard Maristany 16, 08019 Barcelona, Spain

ARTICLE INFO

Keywords:
Hydrogen
Dimethyl ether
Steam reforming
Autothermal reforming
Microreactor
Micromonolith

ABSTRACT

The steam reforming and oxidative steam reforming of dimethyl ether (DME) were tested at 573–773 K over a $CuZn/ZrO_2$ catalyst in microreactors with three different types of channels: ceramic square channels with side lengths of 900 and 400 μm, and silicon microchannels of 2 μm of diameter. The channels were first coated with $ZrOCl_2$ (ceramic channels) or $Zr(i\text{-}PrO)_4$ (silicon microchannels) and calcined at 773 K for 2 h to obtain a homogeneous and well-adhered ZrO_2 layer, as determined by SEM, and then Cu and Zn (Cu:Zn = 1:1 M, 20 wt% total metal) were co-impregnated. Operation at highly reduced residence time (10^{-3} s) while achieving hydrogen yields similar to those recorded over the ceramic channels was possible for the silicon microchannels due to the three orders of magnitude increased contact area. In addition, the amount of catalyst used for coating the silicon microchannels was two orders of magnitude lower with respect to the conventional ceramic channels. Outstanding specific hydrogen production rates of 0.9 L_N of H_2 per min and cm^3 of reactor volume were achieved as well as stable operation for 80 h, which demonstrates the feasibility of using on-site, on-demand hydrogen generation from DME for portable fuel cell applications.

1. Introduction

Dimethyl ether (DME) can be used as a high-density hydrogen carrier facilitating the operation of fuel reformers for feeding low-temperature fuel cells in portable applications due to its low evaporation temperature and its corrosion-safe and easy handling character. The reforming of DME represents an excellent way to feed fuel cells in small environments because DME can be easily stored in liquid form at low pressure (≥0.51 MPa bar at 298 K) and then transformed into gas by a simple pressure relief valve, thus avoiding the need of investing energy for evaporation, as it occurs with other common liquids used for on-board hydrogen generation such as methanol, ethanol, gasoline or diesel [1,2]. In addition, DME can be obtained from almost any carbonaceous feedstock by first generating synthesis gas and then allowing synthesis gas to react over a catalyst [3]. Given the absence of C—C bonds in DME, which can only be cleaved at high temperatures, the catalytic reforming of DME can be carried out at moderate temperatures (573–873 K). Different catalytic reforming technologies can be applied to generate hydrogen from DME (Eq. (1)), being steam reforming (n = 0) and oxidative steam reforming (0 < n < 3) the most appropriate to optimize a trade-off between energy input, hydrogen yield, operation simplicity, and catalyst stability [4–7].

$$CH_3OCH_3 + (3\text{-}n)\ H_2O + n/2\ O_2 \rightarrow (6\text{-}n)\ H_2 + 2\ CO_2 \quad (1)$$

The catalytic reforming of DME at moderate temperature consists of two consecutive reactions; first, DME is hydrolyzed to methanol over an acid catalyst, and then methanol is subsequently transformed into a mixture of H_2 and CO_x over a metal function with the participation of the water gas shift reaction (WGS). Acidity of the catalyst is supplied by the support, usually $\gamma\text{-}Al_2O_3$, ZrO_2, WO_3/ZrO_2 and zeolites such as ZSM-5 [8–23], but also tungstosilicoheteropolyacids, Ga_2O_3/TiO_2 and Mo_2C [24–26], whereas the metal function is usually based on Cu (normally CuZn or Cu/CeO_2) [27–39] or Pd (Pd or PdZn) [40–43], although the use of other metals such as Ni, Pt, Rh, Ru and Au [44–53] and spinel oxides such as $CuFe_2O_4$ have also been described in the literature [54–65]. A proper balance between the metallic and the acid functions is required to guarantee a high hydrogen yield and catalyst stability. Not only the acid amount, but also the acid strength and the type of acid-site definitely affect the steam reforming and hydrolysis activity [10,33,37]. The most used metal for DME steam reforming is copper (as it is the most used for methanol reforming). The interaction of Cu with the support and the distribution of copper species (Cu metal vs. Cu^+)

* Corresponding author at: Institute of Energy Technologies, Universitat Politècnica de Catalunya, EEBE, Eduard Maristany 16, 08019 Barcelona, Spain.
E-mail address: jordi.llorca@upc.edu (J. Llorca).

https://doi.org/10.1016/j.cattod.2018.03.011
Received 16 January 2018; Received in revised form 3 March 2018; Accepted 8 March 2018

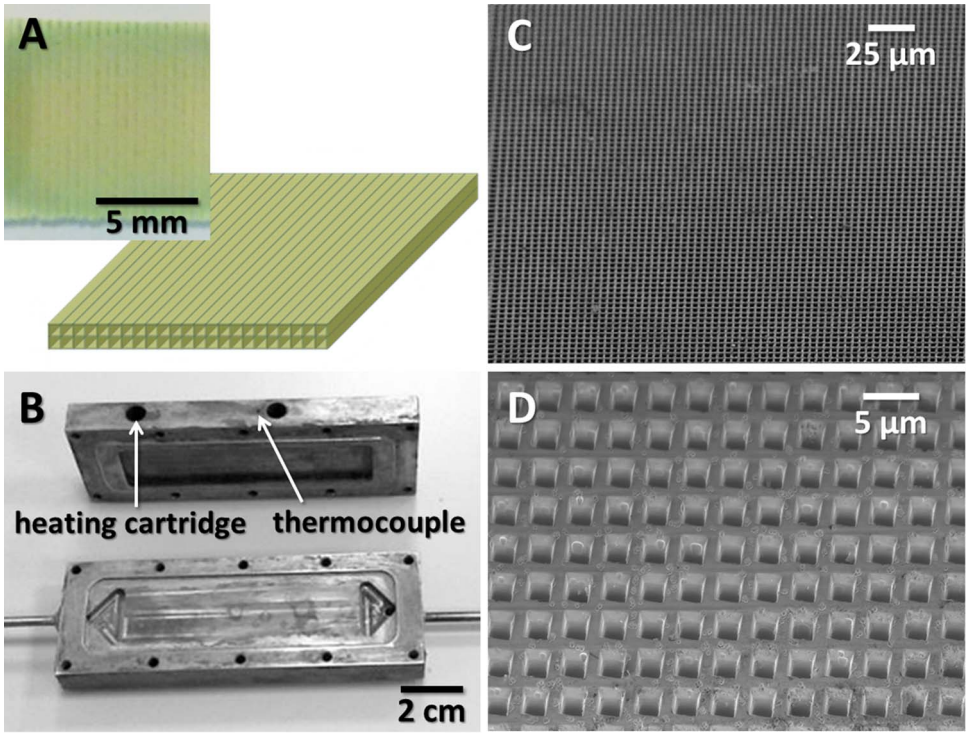

Fig. 1. A) Cordierite honeycomb piece of 900 cpsi (photograph and scheme) coated with $CuZn/ZrO_2$ catalyst. B) Stainless steel microreactor used to test the catalytic cordierite honeycomb structures. C) and D) SEM images of the microchannels of the silicon micromonoliths prepared in this work.

play a determinant role for DME reforming [30,66]. Since Cu nanoparticles tend to sinter under DME reforming conditions Zn is usually added to ensure a robust catalyst [16,30,35–37,46,66–68]. Also, the addition of alkaline elements and alkaline earth metal oxides in the catalyst formulation has been described to have a positive effect, either by modifying the acidity of the support and thus suppressing the formation of undesired hydrocarbons, or by changing the reducibility of the metal function of the catalyst [18,37,53].

For a portable, on-demand fuel reformer, the advantage of oxidative steam reforming over steam reforming is the energy balance of the system. Whereas steam reforming is an endothermic process ($\Delta H^\circ \sim 124$ kJ/mol), oxidative steam reforming can be carried out under autothermal conditions at the expense of hydrogen yield [4,41,50,55,68]. Both the catalytic steam reforming and catalytic oxidative steam reforming of DME have been widely described in the literature. Most of these studies have been addressed towards the formulation of active, selective and stable catalysts and, for practical reasons, powdered catalysts have been generally used. As an additional step in catalyst implementation for real applications a few works have been carried out over catalytic cordierite honeycombs [21,41,42,66–72] as well as microreactors and foams [27,73–78]. Here we extend these studies towards process intensification in DME fuel reformers by using catalytic microstructures containing channels with smaller dimensions. In particular, we study the catalytic performance of cordierite honeycombs with channels of side lengths of 900 and 400 µm and silicon microhoneycombs with microchannels of only 2 µm in diameter coated with $CuZn/ZrO_2$. Lowering the dimensions of the microchannels has a strong effect on the geometric surface area exposed to reactants, which in turn has a dramatic effect on the yield of hydrogen obtained calculated on a volumetric basis [79,80]. Moreover, mass and heat transfer are enhanced and less amount of catalyst is required when decreasing the diameter of the microchannels, in particular for the silicon microhoneycombs.

2. Experimental methods

2.1. Preparation of the catalytic structures

2.1.1. Conventional catalytic honeycombs

Conventional cordierite honeycomb structures of 400 and 900 cpsi (cells per square inch) with square channels with side lengths of 900 and 400 µm, respectively, were first washcoated with an aqueous solution of $ZrOCl_2{\cdot}8\ H_2O$ at 353 K under continuous axial rotation and calcined in air at 773 K for 2 h to obtain a well-adhered layer of ZrO_2 [68]. Then, Cu and Zn were incorporated by a single-step incipient wetness impregnation from an ethanolic solution of $Cu(NO_3)_2{\cdot}3H_2O$ and $Zn(NO_3)_2{\cdot}6H_2O$ (Cu:Zn = 1:1 M, 20 wt% total metal) at room temperature. The resulting catalytic honeycombs were calcined in air at 773 K for 5 h. The acidity values calculated from NH_3-TPD were 0.8 $mmol_{NH3}/g_{catalyst}$. A catalyst loss below 5 wt% was measured during adherence tests in ultrasounds at 40 kHz for 30 min. Honeycombs washcoated only with the ZrO_2 support were used to conduct blank experiments.

2.1.2. Silicon catalytic microhoneycombs

Silicon microhoneycombs were prepared over < 100 > n-type silicon wafers, with a resistivity of 2–6 Ω cm. The channels were manufactured by photoassisted electrochemical etching and subsequent opening of the pores from the back side following the methodology described in [81]. Previously, the wafer surface was prestructured by lithography and etched with tetramethylammonium hydroxide (TMAH) to create a square array of inverted pyramids pointing toward the bulk of the wafer and defining the positions of channel growth. The electrochemical etching was carried out at 288 K at a constant anodic potential of 2 V in 5 wt% HF solution using an array of LEDs with an 880-nm peak emission wavelength. After the electrochemical etching, the wafers were oxidized in O_2 at 1373 K for 30 min, the oxide layer on the backside was removed, and the remaining backside silicon was etched off in 25 wt% TMAH solution at 358 K until the pore tips were reached. The resulting structures were silicon wafers with a thickness of 0.2 mm

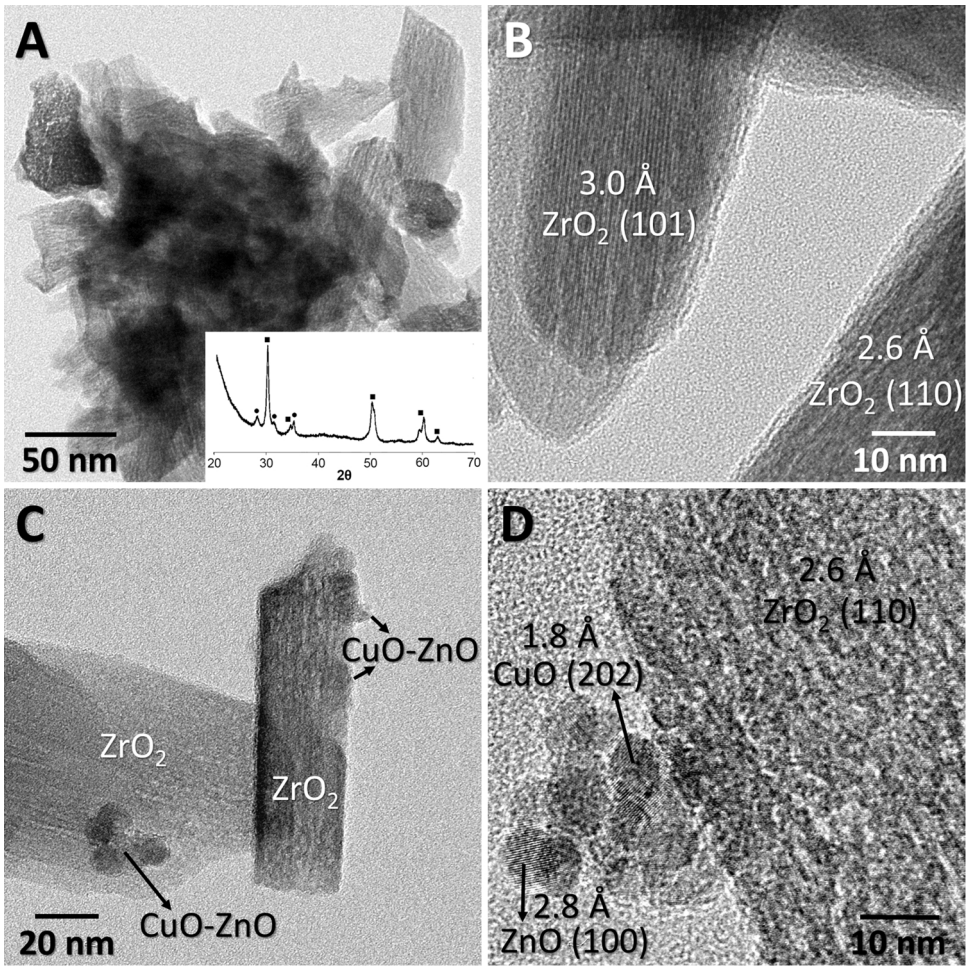

Fig. 2. A) Low-magnification TEM image and XRD pattern of the ZrO_2 support particles (■ tetragonal ZrO_2, ● monoclinic ZrO_2). B) HRTEM image of the support particles showing the characteristic lattice fringes of ZrO_2. C) and D) HRTEM images of the CuZn/ZrO_2 catalyst showing the occurrence of CuO and ZnO nanoparticles.

and with straight microchannels of 2 µm in diameter arranged in a square lattice with a periodicity of 3 µm (Fig. 1C and D), which means ca. 10^7 microchannels/cm^2 and an open frontal area of 35%. An insignificant pressure drop of less than 0.01 bar was measured with nitrogen flowing at 100 mL/min and room temperature. Subsequently, the microchannels were first filled with Zr(i-PrO)$_4$ by applying a pressure gradient of ca. 100 kPa and calcined at 773 K for 2 h to obtain a homogeneous and well-adhered ZrO_2 layer onto the microchannels walls, and then Cu and Zn (Cu:Zn = 1:1 M) were co-impregnated following the same procedure explained above for the conventional catalytic honeycombs. This methodology is based on previous studies where catalytic layers of Co/ZnO, RhPd/CeO_2 and Au/TiO_2 were successfully deposited in silicon microchannels of 3–4 µm in diameter to perform the reforming of ethanol [81–83] and the preferential oxidation of carbon monoxide [84].

2.2. Characterization techniques

Powder X-ray diffraction (XRD) was carried out with a Bruker D8 instrument equipped with a Cu target at a step width of 0.02° and by counting 1 s at each step. Scanning electron microscopy (SEM) images were recorded at 5 kV using a Neon40 Crossbeam Station (Zeiss) instrument equipped with a field emission source. Microstructural characterization by high-resolution transmission electron microscopy (HRTEM) was carried out at 200 kV with a JEOL JEM-2010F electron microscope equipped with a field emission gun. X-ray photoelectron spectroscopy (XPS) was performed with a SPECS system using an Al X-ray source (150 W) and a 9-channel Phoibos detector at a pressure below 10^{-6} Pa. Quantification was carried out using Shirley baselines and Gaussian–Lorentzian lineshapes.

2.3. Catalytic tests

The cordierite honeycombs were cut into pieces of 20 mm width × 23 mm long × 2 mm height to fit into the microreactor used for the experiments (Fig. 1A). The microreactor was built in stainless steel and contained a reaction chamber equipped with two collectors for a proper gas distribution (Fig. 1B). Four heating cartridges were allocated alternately for a homogeneous temperature distribution and a thermocouple was placed at the center of the housing block (Fig. 1B). The silicon microhoneycomb wafer was cut with a laser into a disk measuring 8 mm in diameter and glued with epoxy into a stainless steel washer, which was sealed into a stainless steel tubular reactor and placed inside a furnace. The flowrates of DME and O_2 were adjusted with mass flow controllers and H_2O was dosed using a HPLC Knauer Smartline 100 pump. The effluent of the reactor was monitored on line with an Agilent 3000A micro-GC equipped with PLOT U, Stabilwax and 5 Å Molsieve columns for a complete analysis. Carbon balance closure calculations were always within experimental error (5%). The catalytic devices were first activated with a 10% H_2/Ar mixture at 573 K for 2 h. Then the reaction mixture for DME steam reforming was introduced at this temperature, with a DME:H_2O molar ratio of 1:6 (S/C = 3). The reaction was followed from 573 to 773 K at atmospheric pressure. Oxidative steam reforming was performed at 773 K using a S/C ratio of 3 and a O_2/DME ratio of 0.5. DME conversion (%) is defined as $DME_{conv} = 100n_{DME,conv}/2n_{DME,in}$, where $n_{DME,conv}$ represents the

moles of DME converted measured as the sum of moles of CO_2, CO, CH_4 and CH_3OH at the reactor outlet and $n_{DME,in}$ represents the moles of DME at the reactor inlet. Selectivity to species *i* (%) is calculated as the moles of *i* divided by the total moles of products (H_2, CO_2, CO, CH_4 and CH_3OH), $S_i = 100n_i/\Sigma n_T$. Yield to species *i* (%) is calculated as $Y_i = DME_{conv}S_i/100$.

3. Results and discussion

3.1. Characterization of the catalytic structures

The ZrO_2 support and the $CuZn/ZrO_2$ catalyst deposited on the catalytic cordierite honeycombs walls were characterized by XRD, TEM and XPS after ripping some powder off the walls. A representative, low-magnification TEM image of the ZrO_2 support particles is shown in Fig. 2A. The sample is constituted by crystalline elongated platelets of about 40–100 nm in length. The XRD pattern (Fig. 2A) indicates that most of the support particles are tetragonal ZrO_2, with a minor contribution of monoclinic ZrO_2. This is in accordance with the calcination temperature used during the synthesis [66]. A high resolution TEM image of the ZrO_2 support particles is shown in Fig. 2B. The platelets show well-defined lattice fringes according to their crystalline nature, with crystallographic planes at 3.0 and 2.6 Å, which correspond well to the (101) and (110) planes of tetragonal ZrO_2. Fig. 2C and D show representative TEM images of the $CuZn/ZrO_2$ catalyst prepared by co-impregnating the corresponding Cu and Zn nitrates over the preformed ZrO_2 support particles. In addition to the elongated platelets of the ZrO_2 support, the occurrence of much smaller nanoparticles of about 6–8 nm is clearly seen. An accurate analysis of their lattice fringes observed under HRTEM reveals that they correspond to an intimate mixture of CuO and ZnO nanoparticles. All the nanoparticles analyzed show lattice fringes corresponding to CuO or ZnO. As an example, the crystallographic planes at 1.8 Å of the nanoparticle shown in Fig. 2D are ascribed to the (202) planes of CuO, and those at 2.8 Å are ascribed to the (100) crystallographic planes of ZnO. It should be highlighted that the CuO and ZnO phases appear well mixed and in a narrow size distribution. The XPS surface analysis of the $CuZn/ZrO_2$ catalyst shows a Cu/Zn atomic ratio of 0.87 and a (Cu + Zn)/Zr atomic ratio of 0.41, thus indicating an excellent and homogeneous distribution of both Cu and Zn, in accordance to the HRTEM results.

The characterization of the $CuZn/ZrO_2$ catalyst inside the silicon microchannels was challenging given the small dimensions of the microchannels and the low catalyst loading. For a proper characterization, one of the as-prepared catalytic silicon microhoneycombs was cut and the vertical cross sections of the catalytic microchannels exposed were studied by SEM. Fig. 3 shows a representative view of the catalytic layer on the silicon microchannels. The same area is shown recorded by secondary electrons (Fig. 3A) and backscattered electrons (Fig. 3B). On top the silicon structure a well-developed layer of SiO_2 of about 200 nm in thickness is observed (which was the result of the oxidation treatment at 1373 K for 30 min during the preparation of the silicon microchannels, as explained in Section 2.1.2) and, on top of it, a layer of the ZrO_2 porous support of about 80–100 nm in thickness is recognized. The homogeneity and constant thickness of the ZrO_2 support layer are remarkable. In addition, spherical particles are clearly visible on the ZrO_2 layer; their EDX analyses show the common occurrence of Cu and Zn in all of them. Therefore, it can be assumed that similar catalyst architectures are present in the $CuZn/ZrO_2$ catalytic layers of the cordierite honeycombs and of the silicon microchannels.

3.2. DME steam reforming and oxidative steam reforming

The steam reforming of DME was carried out over the three types of catalytic channels at a constant S/C value of 3 at 573, 623, 673, 723 and 773 K and atmospheric pressure. The data reported here corresponds to steady-state values after 1 h of reaction; no deactivation was

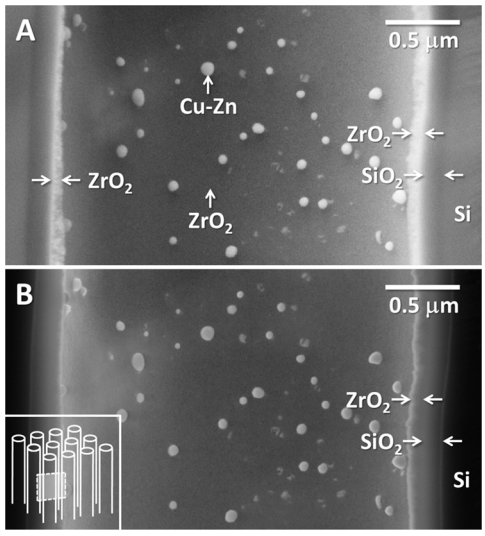

Fig. 3. SEM images recorded using secondary (A) and backscattered (B) electrons of the vertical cross section of an individual microchannel in the silicon microhoneycomb (see the scheme shown in the inset in B). In addition to the Si walls of the silicon structure, layers of SiO_2 and ZrO_2 are clearly identified as well as Cu-Zn nanoparticles anchored on the ZrO_2 support.

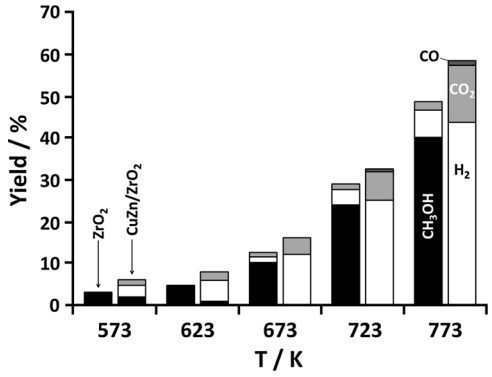

Fig. 4. Product yield obtained with a 900 cpsi cordierite honeycomb loaded with ZrO_2 and $CuZn/ZrO_2$ under DME steam reforming conditions at different temperatures. S/C = 3, $T_{STP} \sim 0.5$ s, GHSV ~ $5{\cdot}10^3\ h^{-1}$. DME conversion corresponds to the height of the bar and product selectivity is represented by the area of each product inside each bar.

observed for any experimental condition assayed. Fig. 4 shows the DME conversion, product selectivity and product yield obtained at each temperature with the cordierite honeycomb structures of 900 cpsi with square channels with side length of 400 µm coated with the bare ZrO_2 support (blank experiment) and with the $CuZn/ZrO_2$ catalyst. In both cases, the conversion of DME increased with temperature, as expected from a thermodynamic point of view taking into account the endothermic character of the process. The main product obtained over the ZrO_2 support was methanol, in accordance to the first step of the reaction (the hydrolysis of dimethyl ether) and the acidic character of ZrO_2. At high temperature, partial steam reforming of methanol into H_2 and CO_2 was observed, particularly at 723 and 773 K. In contrast, the reaction over the $CuZn/ZrO_2$ catalyst yielded exclusively the reforming products at temperatures higher than 673 K (methanol was observed as an intermediate product only at lower temperature). This fact demonstrates the high activity of the CuZn phase for the steam reforming of methanol. At high temperatures, 723 and 773 K, minor amounts of CO are measured in addition to the main products H_2 and CO_2. This is explained taking into account the water gas shift equilibrium: $H_2O + CO \rightleftarrows H_2 + CO_2$. In addition, traces of CH_4 are also measured, probably as a result of the hydrogenation of CO_x.

Exactly the same trends were observed for the cordierite honeycomb

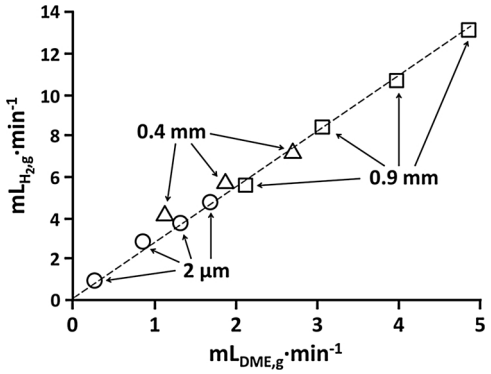

Fig. 5. Hydrogen production rates under DME steam reforming conditions using microchannels coated with $CuZn/ZrO_2$ with different diameters and DME feed flow rates. T = 773 K, S/C = 3, T_{STP} ~ 10^{-3}–1 s, GHSV ~ 10^3–10^5 h^{-1}.

structures of 400 cpsi with square channels with side length of 900 µm in accordance to previous studies [68] and for the silicon micromonoliths coated with the $CuZn/ZrO_2$ catalyst. However, given the differences in their channel dimensions, the spatial conditions tested were different; in particular, the contact time (T_{STP}) varied from 1 ms up to 1 s and the gas hourly space velocity (GHSV) varied from approximately 10^3 to 10^5 h^{-1}. Fig. 5 shows the production of hydrogen (NmL/min) under different DME load values for the three different channel geometries recorded at 773 K. It is remarkable that the hydrogen production values adjust well to a straight line through the origin, which means that the three channel geometries tested behave similarly in the range studied. This is a meaningful result which indicates that process intensification is plausible, even if the contact time is varied by several orders of magnitude. Therefore, an accurate comparison between the three channel geometries is not straightforward and, for that reason, a specific volumetric normalized parameter will be used here, which is defined as the amount of hydrogen generated per amount of DME in the feed (valid in the range used of 0–5 $mL_{DME,g}$/min) for a given reactor volume: $mL_{H2,g}/(mL_{DME,g}\ cm^3_{reactor})$.

The specific volumetric production of hydrogen obtained at 773 K with respect to the channel diameter for the three catalytic structures is shown in Fig. 6A along with the variation of the surface area to volume ratio, m^2/m^3, and the variation of the amount of catalyst weight per surface area, mg_{cat}/cm^2. The inverse relationship between the diameter of the microchannels and the surface area to volume ratio is a direct consequence of the geometry of the catalytic structures. The value of $4{\cdot}10^5$ m^2/m^3 corresponding to the silicon microhoneycomb with straight microchannels of 2 µm in diameter represents nowadays the highest value ever reported for a structured catalytic reactor. The specific volumetric production of hydrogen with respect to the channel diameter follows a similar trend as that observed for the surface area to volume ratio. The smaller the diameter of the microchannel the higher the surface area to volume ratio and the higher the specific volumetric production of hydrogen. In particular, the ca. three order of magnitude difference between the values recorded for the silicon microchannels with respect to the conventional cordierite 400 cpsi honeycombs merits to be highlighted. The parallel trend between the surface area to volume ratio and the specific volumetric production of hydrogen is confirmed in Fig. 6B, where a linear trend between the two parameters is evident. The specific volumetric production of hydrogen values against the geometric surface area to volume ratios adjust well to a straight line through the origin, with an approximate relationship of $mL_{H2,g}/(mL_{DME,g}\ cm^3_{reactor}) = 0.0016\ m^2/m^3$. On the other hand, the amount of catalyst per surface area used in the different catalytic honeycombs is remarkably different, being the amount of catalyst present in the silicon microhoneycomb almost two orders of magnitude lower than those present in the cordierite honeycombs (Fig. 6A and B). This represents an additional advantage of using microchannels with small dimensions

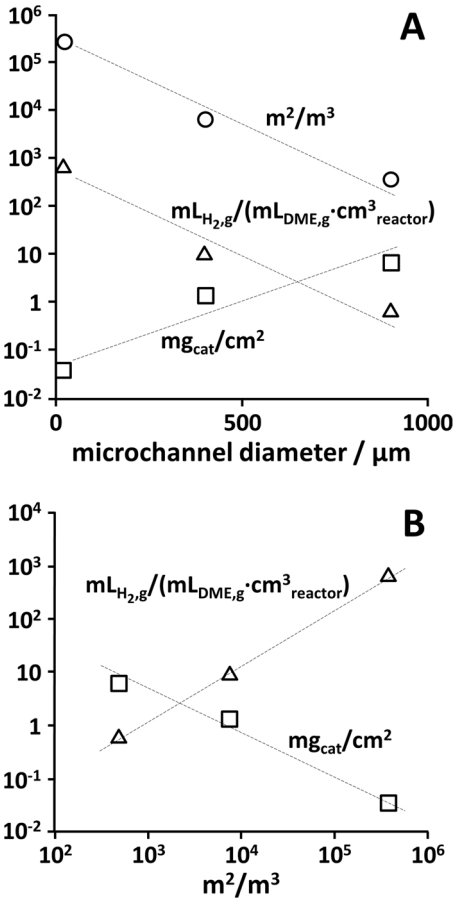

Fig. 6. Variation of surface area to volume ratio (m^2/m^3, ○), catalyst loading per surface area (mg_{cat}/cm^2, □) and specific volumetric production of hydrogen ($mL_{H2,g}/(mL_{DME,g}\ cm^3_{reactor})$, Δ) under DME steam reforming conditions using microchannels coated with $CuZn/ZrO_2$ with different diameters. T = 773 K, S/C = 3, T_{STP} ~ 10^{-3}–1 s, GHSV ~ 10^3–10^5 h^{-1}.

and/or catalytic structures with high surface area to volume ratio for the reforming of DME, which in addition has a beneficial economic impact. Therefore, the use of silicon microhoneycombs with regular channels of 2 µm requires roughly 100 times less catalyst that the conventional cordierite 400 cpsi honeycombs and yields 1000 times more hydrogen on a volumetric basis.

Taking into account the outstanding hydrogen production rate on a volumetric basis of the silicon microhoneycomb with respect to the cordierite honeycombs, a study of the oxidative steam reforming of DME was carried out over the silicon structure at 773 K. The S/C ratio was maintained constant at a value of 3 and the O_2/DME ratio was fixed at a value of 0.5 on a molar basis, which accounts for a slightly exothermic process [4,6]. As expected, the selectivity of H_2 and CO decreased and the selectivity toward CO_2 increased with respect to the DME steam reforming process due to the presence of O_2 in the feed (the selectivity values recorded under DME steam reforming were 74.0% H_2, 23.3% CO_2 and 2.7% CO and those recorded under DME oxidative steam reforming were 66.6% H_2, 28.7% CO_2 and 4.7% CO for a similar DME conversion of ~60%). The hydrogen yield also diminished, decreasing from ca. 44% for DME steam reforming conditions (Fig. 4) to 41% under DME oxidative steam reforming conditions. A stability test was performed for 80 h under DME oxidative steam reforming and an excellent catalytic stability was measured, as shown in Fig. 7. The inspection by SEM and TEM of the catalytic silicon microhoneycomb and the catalyst after ripping some powder off the walls after reaction did not reveal any difference with the fresh structure. Neither carbon deposition nor metal sintering was observed (Fig. 8).

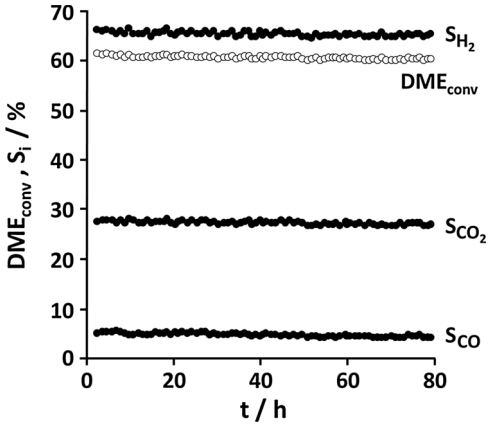

Fig. 7. Product selectivity and DME conversion during a stability test of the silicon microhoneycomb loaded with CuZn/ZrO_2 under DME oxidative steam reforming conditions. T = 773 K, S/C = 3, O_2/DME = 0.5, T_{STP} ~ 1 ms, GHSV ~ $10^5\,h^{-1}$.

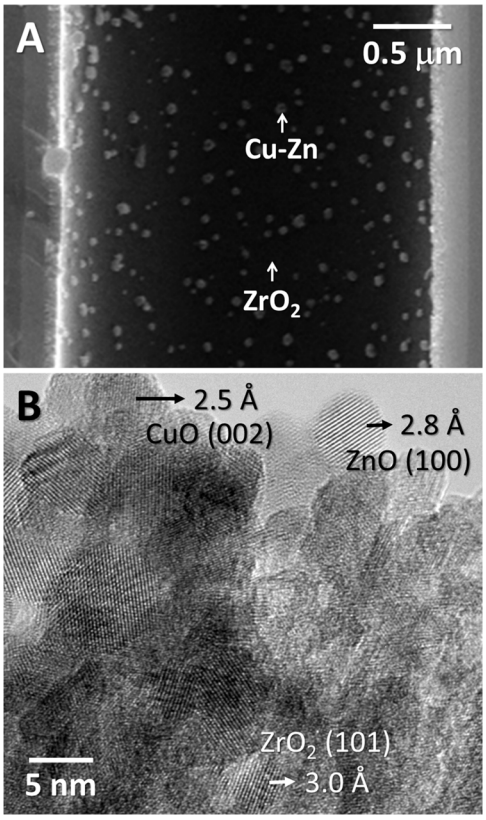

Fig. 8. SEM (A) and TEM (B) images of the catalytic silicon microhoneycomb loaded with the CuZn/ZrO_2 catalyst after a stability test under DME oxidative steam reforming conditions for 80 h.

4. Conclusions

Catalytic wall honeycombs consisting of ceramic cordierite channels with side lengths of 900 and 400 μm and silicon disks containing ca. 10^7 microchannels of 2 μm of diameter per cm^2 have been successfully coated with a homogeneous layer of CuZn/ZrO_2 catalyst by a two-step process. First, a support layer of ZrO_2 has been adhered onto the channels walls, and then Cu and Zn have been co-impregnated. A thin catalyst layer of 80–100 nm in thickness has been grafted onto the silicon microchannels, which has resulted in a two order of magnitude less amount of catalyst per surface area with respect to the conventional cordierite honeycombs (0.03 vs. 1.5–6 $mg_{catalyst}/cm^2$, respectively). Besides, given the small dimension of the silicon microchannels, the surface area to volume ratio of the silicon disks has exceeded in various orders of magnitude that of the conventional cordierite honeycombs ($4{\cdot}10^5$ vs. $5{\cdot}10^2$–$8{\cdot}10^3$ m^2/m^3, respectively). As a direct consequence of both factors, the catalytic silicon microstructures have performed much better in terms of specific hydrogen production rates in the steam reforming of DME at 573–773 K (S/C = 3, GHSV = 10^3–$10^5\,h^{-1}$), with remarkable specific hydrogen production rates of 0.9 L_N of H_2 per min and cm^3 of reactor volume. To improve the energy balance of the system, the oxidative steam reforming of DME has been also tested at 773 K with O_2/DME = 0.5 over the silicon microchannels. It should be mentioned that the energetic cost of preheating and evaporating the surplus water used in our experiments (S/C = 3) should be considered in conjunction with the conclusions arising from the reaction performance for the final selection of the optimum operational S/C value. The implementation of catalytic silicon microchannels for on-site, on-demand hydrogen generation from DME steam reforming and oxidative steam reforming processes appears promising for portable fuel cell applications.

Acknowledgments

This work has been funded by MINECO/FEDER project ENE2015-63969-R. JL is a Serra Húnter Fellow and is grateful to ICREA Academia program. We are grateful to Pau Solano for technical assistance.

References

[1] D. Li, X. Li, J. Gong, Chem. Rev. 116 (2016) 11529–11653.
[2] Z. Azizi, M. Rezaeimanesh, T. Tohidian, M.R. Rahimpour, Chem. Eng. Process. 82 (2014) 150–172.
[3] J. Sun, G. Yang, Y. Yoneyama, N. Tsubaki, ACS Catal. 4 (2014) 3346–3356.
[4] K. Faungnawakij, N. Viriya-Empikul, W. Tanthapanichakoon, Int. J. Hydrogen Energy 36 (2011) 5865–5874.
[5] T.A. Semelsberger, R.L. Borup, J. Power Sources 152 (2005) 87–96.
[6] T.A. Semelsberger, R.L. Borup, J. Power Sources 155 (2006) 340–352.
[7] K. Faungnawakij, R. Kikuchi, K. Eguchi, J. Power Sources 164 (2007) 73–79.
[8] K. Takeishi, H. Suzuki, Appl. Catal. A: Gen. 260 (2004) 111–117.
[9] T. Nishiguchi, K. Oka, T. Matsumoto, H. Kanai, K. Utani, S. Imamura, Appl. Catal. A: Gen. 301 (2006) 66–74.
[10] K. Faungnawakij, Y. Tanaka, N. Shimoda, T. Fukunaga, S. Kawashima, R. Kikuchi, K. Eguchi, Appl. Catal. A: Gen. 304 (2006) 40–48.
[11] T. Kawabata, H. Matsuoka, T. Shishido, D. Li, Y. Tian, T. Sano, K. Takehira, Appl. Catal. A: Gen. 308 (2006) 82–90.
[12] K. Oka, T. Nishiguchi, H. Kanai, K. Utani, S. Imamura, Appl. Catal. A: Gen. 309 (2006) 187–191.
[13] T.A. Semelsberger, K.C. Ott, R.L. Borup, H.L. Greene, Appl. Catal. A: Gen. 309 (2006) 210–223.
[14] K. Faungnawakij, R. Kikuchi, T. Matsui, T. Fukunaga, K. Eguchi, Appl. Catal. A: Gen. 333 (2007) 114–121.
[15] A.G. Gayubo, J. Vicente, J. Ereña, L. Oar-Arteta, M.J. Azkoiti, M. Olazar, J. Bilbao, Appl. Catal. A: Gen. 483 (2014) 76–84.
[16] Z. Sun, M. Meng, L. Zhang, Y. Zha, X. Zhou, Z. Jiang, S. Zhang, Y. Huang, Int. J. Hydrogen Energy 37 (2012) 18860–18869.
[17] J. Ereña, J. Vicente, A.T. Aguayo, A.G. Gayubo, M. Olazar, J. Bilbao, Int. J. Hydrogen Energy 38 (2013) 10019–10028.
[18] J. Vicente, A.G. Gayubo, J. Ereña, A.T. Aguayo, M. Olazar, J. Bilbao, Appl. Catal. B: Environ. 130–131 (2013) 73–83.
[19] X. Long, Q. Zhang, Z.T. Liu, P. Qi, J. Lu, Z.W. Liu, Appl. Catal. B: Environ. 134–135 (2013) 381–388.
[20] D. Feng, Y. Wang, D. Wang, J. Wang, Chem. Eng. J. 146 (2009) 477–485.
[21] C. Ledesma, J. Llorca, Chem. Eng. J. 154 (2009) 281–286.
[22] J. Li, Q.J. Zhang, X. Long, P. Qi, Z.T. Liu, Z.W. Liu, Chem. Eng. J. 187 (2012) 299–305.
[23] S. Zhou, K. Ma, Y. Tian, M. Meng, T. Ding, Y. Zha, T. Zhang, X. Li, RSC Adv. 6 (2016) 52411–52420.
[24] V.V. Galvita, G.L. Semin, V.D. Belyaev, T.M. Yurieva, V.A. Sobyanin, Appl. Catal. A: Gen. 216 (2001) 85–90.
[25] T. Mathewa, Y. Yamada, A. Ueda, H. Shioyama, T. Kobayashi, C.S. Gopinath, Appl. Catal. A: Gen. 300 (2006) 58–66.
[26] F. Solymosi, R. Barthos, A. Kecskeméti, Appl. Catal. A: Gen. 350 (2008) 30–37.
[27] R. Kousar, D.H. Kim, B.Y. Yu, H.P. Ha, S.H. Kim, J.Y. Byun, Appl. Catal. A: Gen. 423–424 (2012) 176–184.
[28] S. Park, B. Choi, H. Kim, Y.J. Lee, Appl. Catal. A: Gen. 437–438 (2012) 173–183.
[29] K. Takeishi, Y. Akaike, Appl. Catal. A: Gen. 510 (2016) 20–26.
[30] X. Wang, K. Ma, L. Guo, Y. Tian, Q. Cheng, X. Bai, J. Huang, T. Ding, X. Li, Appl. Catal. A: Gen. 540 (2017) 37–46.
[31] X. Zhou, M. Meng, Z. Sun, Q. Li, Z. Jiang, Chem. Eng. J. 174 (2011) 400–407.

[32] S.D. Badmaev, P.V. Snytnikov, Int. J. Hydrogen Energy 33 (2008) 3026–3030.
[33] X. Wang, X. Pan, R. Lin, S. Kou, W. Zou, J.X. Ma, Int. J. Hydrogen Energy 35 (2010) 4060–4068.
[34] P.V. Snytnikov, S.D. Badmaev, G.G. Volkova, D.I. Potemkin, M.M. Zyryanova, V.D. Belyaev, V.A. Sobyanin, Int. J. Hydrogen Energy 37 (2012) 16388–16396.
[35] L. Oar-Arteta, A. Remiro, J. Vicente, A.T. Aguayo, J. Bilbao, A.G. Gayubo, Fuel Process. Technol. 126 (2014) 145–154.
[36] L. Zhang, M. Meng, S. Zhou, Z. Sun, J. Zhang, Y. Xie, T. Hu, J. Power Sources 232 (2013) 286–296.
[37] J. Ereña, J. Vicente, A.T. Aguayo, M. Olazar, J. Bilbao, A.G. Gayubo, Appl. Catal. B: Environ. 142–143 (2013) 315–322.
[38] Y. Zang, X. Dong, C. Wang, Chem. Eng. J. 313 (2017) 1583–1592.
[39] S. Park, H. Kim, B. Choi, Catal. Today 164 (2011) 240–245.
[40] H. Yoshida, N. Iwasa, H. Akamatsu, M. Arai, Int. J. Hydrogen Energy 40 (2015) 5624–5627.
[41] M. Nilsson, K. Jansson, P. Jozsa, L.J. Pettersson, Appl. Catal. B: Environ. 86 (2009) 18–26.
[42] C. Ledesma, U.S. Ozkan, J. Llorca, Appl. Catal. B: Environ. 101 (2011) 690–697.
[43] E. Ramos, L. Davin, I. Angurell, C. Ledesma, J. Llorca, ChemCatChem 7 (2015) 2179–2187.
[44] Q. Zhang, X. Li, K. Fujimoto, K. Asami, Appl. Catal. A: Gen. 288 (2005) 169–174.
[45] N. Laosiripojana, S. Assabumrungrat, Appl. Catal. A: Gen. 320 (2007) 105–113.
[46] T. Fukunaga, N. Ryumon, S. Shimazu, Appl. Catal. A: Gen. 348 (2008) 193–200.
[47] A. Gazsi, I. Ugrai, F. Solymosi, Appl. Catal. A: Gen. 391 (2011) 360–366.
[48] Y. Yamada, T. Mathew, A. Ueda, H. Shioyama, T. Kobayashi, Appl. Surf. Sci. 252 (2006) 2593–2597.
[49] C. Herrera, M.A. Larrubia, P. Kowalik, I.S. Pieta, L.J. Alemany, Int. J. Hydrogen Energy 41 (2016) 19781–19788.
[50] S. Choi, J. Bae, J. Power Sources 307 (2016) 351–357.
[51] Q. Zhang, F. Du, X. He, Z.T. Liu, Z.W. Liu, Y. Zhou, Catal. Today 146 (2009) 50–56.
[52] O. Mihai, A. Fathali, X. Auvray, L. Olsson, Appl. Catal. B: Environ. 160–161 (2014) 480–491.
[53] J. Li, Q. Zhang, Y. Zhao, P. Qi, C. Shao, React. Kinet. Mech. Catal. 122 (2017) 1193–1202.
[54] K. Faungnawakij, N. Shimoda, T. Fukunaga, R. Kikuchi, K. Eguchi, Appl. Catal. A: Gen. 341 (2008) 139–145.
[55] K. Faungnawakij, N. Viriya-Empikul, Appl. Catal. A: Gen. 382 (2010) 21–27.
[56] K. Faungnawakij, R. Kikuchi, T. Fukunaga, K. Eguchi, Catal. Today 138 (2008) 157–161.
[57] K. Faungnawakij, Y. Tanaka, N. Shimoda, T. Fukunaga, R. Kikuchi, K. Eguchi, Appl. Catal. B: Environ. 74 (2007) 144–151.
[58] K. Eguchi, N. Shimoda, K. Faungnawakij, T. Matsui, R. Kikuchi, S. Kawashima, Appl. Catal. B: Environ. 80 (2008) 156–167.
[59] K. Faungnawakij, N. Shimoda, T. Fukunaga, R. Kikuchi, K. Eguchi, Appl. Catal. B: Environ. 92 (2009) 341–350.
[60] K. Faungnawakija, N. Shimoda, N. Viriya-Empikul, R. Kikuchi, K. Eguchi, Appl. Catal. B: Environ. 97 (2010) 21–27.
[61] L. Oar-Arteta, A. Remiro, A.T. Aguayo, J. Bilbao, A.G. Gayubo, Ind. Eng. Chem. Res. 54 (2015) 9722–9732.
[62] L. Oar-Arteta, A.T. Aguayo, A. Remiro, J. Bilbao, A.G. Gayubo, Ind. Eng. Chem. Res. 54 (2015) 11285–11294.
[63] L. Oar-Arteta, A. Remiro, F. Epron, N. Bion, A.T. Aguayo, J. Bilbao, A.G. Gayubo, Ind. Eng. Chem. Res. 55 (2016) 3546–3555.
[64] L. Oar-Arteta, A. Remiro, A.T. Aguayo, M. Olazar, J. Bilbao, A.G. Gayubo, RSC Adv. 6 (2016) 52411–52420.
[65] K. Faungnawakij, R. Kikuchi, T. Fukunaga, K. Eguchi, J. Phys. Chem. C 113 (2009) 18455–18458.
[66] C. Ledesma, J. Llorca, J. Phys. Chem. C 115 (2011) 11624–11632.
[67] M. Nilsson, L.J. Pettersson, B. Lindström, Energy Fuel 20 (2006) 2164–2169.
[68] C. Ledesma, J. Llorca, Fuel 104 (2013) 711–716.
[69] S. Park, H. Kim, B. Choi, J. Ind. Eng. Chem. 16 (2010) 734–740.
[70] M. Nilsson, P. Jozsa, L.J. Pettersson, Appl. Catal. B: Environ. 76 (2007) 42–50.
[71] S. Park, B. Choi, B.S. Oh, Int. J. Hydrogen Energy 36 (2011) 6422–6432.
[72] S. Jung, B. Choi, S. Park, D.W. Lee, Y.B. Kim, Int. J. Hydrogen Energy 42 (2017) 13463–13476.
[73] M. Yang, Y. Men, S. Li, G. Chen, Appl. Catal. A: Gen. 433–434 (2012) 26–34.
[74] M. Yang, Y. Men, S. Li, G. Chen, Int. J. Hydrogen Energy 37 (2012) 8360–8369.
[75] C.F. Yan, W. Ye, C.Q. Guo, S.L. Huang, W.B. Li, W.M. Luo, Int. J. Hydrogen Energy 39 (2014) 18642–18649.
[76] C. Yan, H. Hai, R. Hu, C. Guo, S. Huang, W. Li, Y. Wen, Int. J. Hydrogen Energy 39 (2014) 18625–18631.
[77] C. Yan, H. Hai, C. Guo, W. Li, S. Huang, H. Chen, Int. J. Hydrogen Energy 39 (2014) 10409–10416.
[78] D.H. Kim, S.H. Kim, J.Y. Byun, Chem. Eng. J. 280 (2015) 468–474.
[79] I. Uriz, G. Arzamendi, E. López, J. Llorca, L.M. Gandía, Chem. Eng. J. 167 (2011) 603–609.
[80] A. Casanovas, M. Domínguez, C. Ledesma, E. López, J. Llorca, Catal. Today 143 (2009) 32–37.
[81] J. Llorca, A. Casanovas, T. Trifonov, A. Rodríguez, R. Alcubilla, J. Catal. 255 (2008) 228–233.
[82] N.J. Divins, E. López, A. Rodríguez, D. Vega, J. Llorca, Chem. Eng. Process. Process Intensif. 64 (2013) 31–37.
[83] E. López, A. Irigoyen, T. Trifonov, A. Rodríguez, J. Llorca, Int. J. Hydrogen Energy 35 (2010) 3472–3479.
[84] N.J. Divins, E. López, M. Roig, T. Trifonov, A. Rodríguez, F. González de Rivera, L.I. Rodríguez, M. Seco, O. Rossell, J. Llorca, Chem. Eng. J. 167 (2011) 597–602.